Article

3-D Residual Eddy Current Field Characterisation: Applied to Diffusion Weighted Magnetic Resonance Imaging

O'BRIEN, Kieran, *et al*.

O'BRIEN, Kieran, *et al*. 3-D Residual Eddy Current Field Characterisation: Applied to Diffusion Weighted Magnetic Resonance Imaging. *IEEE Transactions on Medical Imaging*, 2013, vol. 32, no. 8, p. 1515-1525

DOI : 10.1109/TMI.2013.2259249
PMID : 23674437

3-D Residual Eddy Current Field Characterisation: Applied to Diffusion Weighted Magnetic Resonance Imaging

Kieran O'Brien*, Alessandro Daducci, Nils Kickler, Francois Lazeyras, Rolf Gruetter, Thorsten Feiweier, and Gunnar Krueger

***Abstract*—Clinical use of the Stejskal–Tanner diffusion weighted images is hampered by the geometric distortions that result from the large residual 3-D eddy current field induced. In this work, we aimed to predict, using linear response theory, the residual 3-D eddy current field required for geometric distortion correction based on phantom eddy current field measurements. The predicted 3-D eddy current field induced by the diffusion-weighting gradients was able to reduce the root mean square error of the residual eddy current field to ~1 Hz. The model's performance was tested on diffusion weighted images of four normal volunteers, following distortion correction, the quality of the Stejskal–Tanner diffusion-weighted images was found to have comparable quality to image registration based corrections (FSL) at low b-values. Unlike registration techniques the correction was not hindered by low SNR at high b-values, and results in improved image quality relative to FSL. Characterization of the 3-D eddy current field with linear response theory enables the prediction of the 3-D eddy current field required to correct eddy current induced geometric distortions for a wide range of clinical and high b-value protocols.**

***Index Terms*—Brain, diffusion, eddy currents, magnetic resonance imaging (MRI), tractography.**

Manuscript received March 18, 2013; accepted April 08, 2013. Date of publication May 06, 2013; date of current version July 27, 2013. This work was supported by the Centre d'Imagerie BioMédicale (CIBM) of the UNIL, UNIGE, HUG, CHUV and EPFL, the Leenaards and Louis-Jeantet foundations. *Asterisk indicates corresponding author.*

*K. O'Brien is with the Department of Radiology, University of Geneva, 1211 Geneva, Switzerland and the Advanced Clinical Imaging Technology, CIBM-Siemens Suisse SA, 1015 Lausanne, Switzerland (e-mail: kieran.obrien@epfl.ch).

A. Daducci is with the Signal Processing Lab (LTS5), Ecole Polytechnique Fédérale de Lausanne, 1015 Lausanne, Switzerland (e-mail: alessandro.daducci@epfl.ch).

N. Kickler was with Laboratory of Functional Metabolic Imaging, Ecole Polytechnique Fédérale de Lausanne, 1015 Lausanne, Switzerland. He is now with Bosch GmbH, 70442 Stuttgart, Germany (e-mail: nilskickler@web.de).

F. Lazeyras is with the Department of Radiology, University of Geneva, Geneva, Switzerland (e-mail: francois.lazeyras@unige.ch).

R. Guretter is with the Department of Radiology, University of Geneva, 1211 Geneva, Switzerland: the Laboratory of Functional Metabolic Imaging, Ecole Polytechnique Fédérale de Lausanne, 1015 Lausanne, Switzerland: and, the Department of Radiology, University of Lausanne, 1011 Lausanne, Switzerland, (e-mail: rolf.gruetter@epfl.ch).

T. Feiweier is with Siemens AG, Healthcare Sector, 91052 Erlangen, Germany (e-mail: thorsten.feiweier@siemens.com).

G. Krueger is with Advanced Clinical Imaging Technology, CIBM-Siemens Suisse SA, 1015 Lausanne, Switzerland (e-mail: gunnar.krueger@siemens.com).

Color versions of one or more of the figures in this paper are available online at http://ieeexplore.ieee.org.

Digital Object Identifier 10.1109/TMI.2013.2259249

I. Introduction

IN MAGNETIC resonance imaging (MRI) a variety of different artefacts result from the induction of eddy currents during gradient switching. Though modern scanners employ several mechanisms to mitigate eddy currents, including gradient design, shielding, and gradient waveform pre-emphasis [1]–[5], certain applications such as diffusion weighted (DW) echo planar imaging (EPI) and phase contrast flow imaging remain particularly sensitive to residual eddy current fields.

Unlike other imaging trajectories, EPI has an inherently low bandwidth per pixel in the phase-encoding direction, which makes it particularly susceptible to geometric image distortion from residual eddy current fields [6], [7]. In particular, the strong gradients required to produce diffusion-weighting still induce residual direction-dependent eddy current fields that may result in significant geometric distortion resulting in misregistrations between the different diffusion-weighted b-values and/or directions that are required to evaluate diffusion-weighted parameters. The errors manifest themselves as regions of artificially altered apparent diffusion coefficients (ADC) or fractional anisotropy (FA) [6]. Both ADC and FA are often used parameters in clinical diagnosis and alterations in those metrics may lead to misleading results.

To overcome the geometric distortion, Papadikis [5] investigated the possibility of establishing a diffusion-weighted specific gradient pre-emphasis procedure, but the result may adversely affect the other gradient pulses within the sequence. Alternatively, if the total acquisition time is not a limiting factor and/or multiple averages are required, then reversing the polarity of the diffusion-weighted gradients [8] or the phase-encoding direction [9], between data sets has been shown to reduce the effect of higher order eddy currents provided an initial linear co-registration step is performed. Yet, clinically, total acquisition time is a critical factor.

To mitigate eddy currents in the acquisition, Reese *et al.* [10], [11] modified the Stejskal–Tanner sequence [12] such that the eddy currents induced by switching the gradients cancel at the time of echo formation, at the expense of the minimum echo time (TE). The twice-refocused spin echo (TRSE) diffusion-encoding scheme reduces the geometric distortion; however, increasing the spatial resolution or use of stronger diffusion-weightings can make the longer TE and subsequent T2 signal loss undesirable [13]. The appeal to return to the Stejskal–Tanner sequence reinitiates the need of alternative

techniques to compensate or correct for the eddy current-related geometric distortion.

Provided that residual eddy current fields remain and that they are constant during the EPI readout, the geometric distortion consists of displacement in the phase encode direction by a distance proportional to the local eddy current field. Image registration approaches that are restricted to the theoretical geometric distortions [14] can retrospectively quantify and correct for the eddy currents. Image registration based eddy current estimation has been shown to have good performance for b-values up to 1000 s/mm^2[15]–[17]. At higher b-values (> 1000 s/mm^2), the greater signal attenuation and the increased sensitivity to diffusion aniosotropy between the different directions makes it more difficult to register these images correctly [18].

Alternatively if the spatial and temporal evolutions of the eddy current fields are known or measured [19], the geometric distortions can be corrected in k-space by regridding from the deformed to an undeformed k-space grid [20], [21] or in image space using the calculated pixel deformation maps [22]. For an ideal correction of the geometric distortion, the eddy current field has to be known at each voxel position in the volume for all the diffusion encoding gradients (direction and amplitude) applied. Truong *et al.* [23] recently proposed acquiring 2-D eddy current field maps on a phantom prior to the *in vivo* acquisition; however, for the large diffusion-weighted-EPI data sets (> 30 directions) desired for diffusion tensor, high angular resolution diffusion imaging [24] and spectrum imaging or for large image volumes (> 20 slices) this procedure would become cumbersome and would be limited to a specific parameter choice of the diffusion-weighted imaging protocol.

Current eddy current measurement techniques are too time intensive to be performed on every patient or they require additional expertise and hardware that limit their clinical application [25], [26]. To avoid time intensive eddy current field measurements we propose to show how linear response theory [27] can be used to temporally and spatially characterize the eddy current field [28]. As an example, linear response theory was used to estimate the residual eddy current field of each b-value and direction of typical diffusion weighted imaging protocols. Correction with the estimated field map was compared to the commonly used FSL's "eddy_correct" algorithm.

II. Materials and Methods

A. Eddy Current Field Characterization

An eddy current field is generated by each gradient ramp in the pulse sequence, whose strength is dependent on the slewrate and the duration of the ramp. In a diffusion weighted acquisition, one can assume that the residual eddy current field has a fixed and variable component. The fixed component comes from gradient events that are present in every acquisition e.g., the EPI and the variable component is due to the diffusion-weighting gradients which change as a function of the b-value and direction applied. In diffusion weighted imaging the artefacts relate to different spatial distortions between directions and b-values, therefore, one only needs to consider their variable contribution to the eddy current field. The sequence is designed such that for fixed acquisition parameters (i.e., field-of-view, matrix size, TE, etc.), the shape of the diffusion gradients stays constant. Thus, when changing the b-value, it is only the amplitude of the diffusion encoding gradients that changes, while their respective duration and ramp times are kept identical. Considering a mono exponential eddy current model [28], which focuses on the long time constants (τ_C) relevant for the spatial distortions investigated here, the induced field perturbation will scale linearly [29] with the change in gradient amplitude (ΔG)

$$EC(t) = \Delta G \exp(\frac{t-T}{\tau_C}) \tag{1}$$

where T is the location of the gradient ramp in time (t).

Equation (1) describes the temporal characteristics, if one considers that the residual eddy current field is slowly varying and free of electric currents, then the spatial description of the eddy current field should obey Laplace's equation and is well described through the use of a spherical harmonic expansion [19], expressed in spherical coordinates (r,ϕ ,θ) as

$$EC(r,\phi,\vartheta) = \sum_{n=0}^{\infty}\sum_{m=0}^{n}\left(\frac{r}{R}\right)^n P_n^m(\cos\vartheta) \left[A_n^m\cos(m\phi) + B_n^m\sin(m\phi)\right] \tag{2}$$

where is the radius of the bore, P_n^m are the fully normalized associated Legendre polynomials and A_n^m, B_n^m are the spherical harmonic coefficients of degree m and order n. The spherical harmonic coefficients scale with ΔG . Therefore, using linear response theory, A_n^m, B_n^m can be replaced with an expression that describes the measured eddy current field as a linear sum of the contribution from each preceding gradient ramp, denoted by subscript i, and on each gradient coil, denoted by subscript j

$$\begin{aligned} A_n^m(t) &= \sum_i \sum_{j=X,Y,Z} a_{nm}^j \Delta G_i^j \exp(\frac{t-T_i}{\tau_C^j}) \\ B_n^m(t) &= \sum_i \sum_{j=X,Y,Z} b_{nm}^j \Delta G_i^j \exp(\frac{t-T_i}{\tau_C^j}) \end{aligned} \tag{3}$$

where a_{nm}^j, b_{mn}^j are the linear coefficients relating ΔG to the eddy current field's strength. Substituting (3) into (2) allows the eddy current field of any arbitrary diffusion-weighted gradient direction or strength to be described [28]

$$\begin{aligned} EC(r,\phi,\vartheta,t) = \sum_{n=0}^{\infty}\sum_{m=0}^{n}\left(\frac{r}{R}\right)^n P_n^m(\cos\vartheta) \Bigg[&\sum_i \sum_{j=X,Y,Z} a_{nm}^j \Delta G_i^j \exp(\frac{t-T_i}{\tau_C^j})\cos(m\phi) \\ &+ \sum_i \sum_{j=X,Y,Z} b_{nm}^j \Delta G_i^j \exp(\frac{t-T_i}{\tau_C^j})\sin(m\phi) \Bigg]. \end{aligned} \tag{4}$$

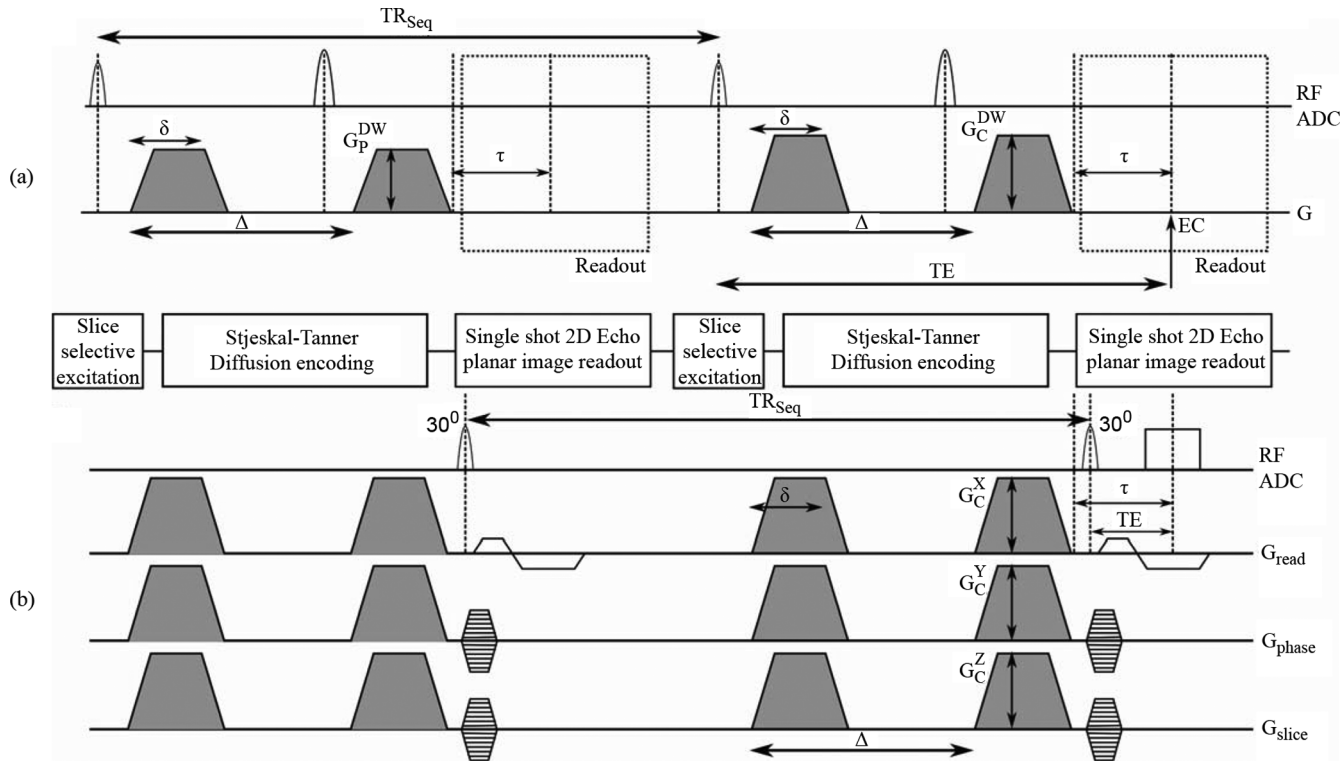

Fig. 1. Schematic representation of a diffusion-weighted-EPI sequence and the 3-D eddy current field mapping sequence. Diffusion-weighting gradient test pulses' timing and amplitude (shaded) in the eddy current field measurement sequence (b) are matched against gradients from the typical diffusion-weighted gradients of the diffusion weighted sequence (a).

B. Eddy Current Field Measurement

The eddy current fields remaining on the compensated system were measured on a 190-mm spherical imaging phantom using the sequence shown in Fig. 1. In 2-D a slice selective or in 3-D a nonselective RF pulse with either a 2-D or 3-D gradient-echo readout follows the test diffusion-weighting gradients at a delay τ. The phase of each voxel $(\Delta\phi)$, averaged over the TE, is representative of the eddy current field at a delay τ after the diffusion-weighting gradients. Any phase alterations caused by other gradients (e.g., slice selection) [4] are removed by subtracting the phase accrued of a second identical volume acquired with no diffusion-weighting gradients. Given the TE, the diffusion-weighting gradient's average eddy current field at each position in space can be calculated as

$$\overline{EC(x,y,z)} = \frac{\Delta\phi(x,y,z)}{\gamma TE}. \tag{5}$$

Image reconstruction of the 3-D eddy current field $\overline{EC(x,y,z)}$ was performed offline using customized Matlab scripts (The MathWorks Inc., South Natick, MA, USA). An isotropic resolution of 8 mm ($32 \times 32 \times 32$ voxels, FOV of 25.6 cm) was found to adequately capture the eddy current field in a reasonable acquisition time. A repetition time (TR) of 150 ms, unless stated, was consistent with the sequence repetitions, the delay between the excitation of subsequent slices in a clinical diffusion-weighted EPI experiment. TE was fixed at 20 ms to obtain a good range of phase accrued $(\Delta\overline{EC(x,y,z)}$ while avoiding discontinuities due to wrapping. Remaining discontinuities, if any, were removed using an unwrapping algorithm based on a weighted least squares solution to Poisson's equation using a specific form of the fast cosine transform [30]. This algorithm was shown to be more robust to noise and data inconsistencies or degradations than path following algorithms [30].

To investigate the time constant of the residual eddy current field, and to ascertain there was no spatial dependence of the time constant, the 2-D eddy current measurement sequence was used to acquire a slice at isocenter orthogonal to the applied diffusion-weighting gradient at different delays. These phantom measurements were used to determine the eddy current decay time constant for each gradient axis.

To fully characterize the effect of changes to the DW gradient pulses on the induced eddy current fields, various diffusion-weighting gradient pulse shapes, amplitudes and temporal delays were examined, summarized in Table I, with the 3-D version of the sequence on a phantom.

1) The dependence on gradient amplitude was assessed by applying diffusion-weighting gradients along each of the three principal gradient axis at different b-values.
2) The superposition of the eddy current fields induced from different gradient coils was examined with three oblique diffusion-weighting gradients.
3) The shape of the diffusion-weighting gradient pulse was considered by varying the gradient amplitude, separation time (Δ), and duration (δ). The aim was to simulate the effect of changing the partial Fourier ratio or image resolution on the available time to play out a diffusion-weighting

TABLE I
MODIFICATION OF DIFFUSION PARAMETERS FOR EDDY CURRENT FIELD MEASUREMENTS

Experiment	δ (ms)	Δ (ms)	TR (ms)	τ (ms)	G^{DW}/G_{ref}*	Equivalent b-value
eddy current decay time constant	36.7	47.9	1000	45 70 95 120 170 200	0.71	1000
Principal axis	36.7	47.9	150	22	0.32 0.45 0.55 0.71 0.87 1.00	250 500 750 1000 1500 2000
Oblique axis	36.7	47.9	150	22	0.45/0.45/-0.32 0.45/-0.32/0.45 0.45/-0.32/0.45	1000
Diffusion-weighted gradient shape	36.7 32.7 29.2	47.9 49.9 52.4	150	22	0.71 0.76 0.81	1000
Eddy current history	36.7	47.9	120 150 180 210	22	1.00	2000
Eddy current decay across readout	36.7	47.9	150	20 22 27 32 37 42	0.71	1000

* Oblique diffusion direction are normalised to $G_{ref,}$ the max gradient applied

gradients along the X-axis, the gradient amplitude was chosen to maintain an equivalent b-value of 1000 s/mm^2.

4) The 3-D eddy current field history, i.e., carry over from previously applied diffusion-weighting gradients was tested by varying the TR with diffusion-weighting gradients applied along the X-axis.
5) The effect of the eddy current field's decay was investigated by varying the time delays (τ), between the diffusion-weighting gradients applied along the X-axis and the 3-D gradient echo acquisition.

The other imaging parameters for the eddy current field map experiments are shown in Table II.

C. Geometric Distortion

To remove the geometric distortion the eddy current field was treated as time invariant over the EPI readout. We chose to predict the eddy current field at the TE by considering the gradient ramps of the diffusion-weighting preceding that point. To determine the unknown weights a^j_{nm} and b^j_{nm} required in (4), a system of linear equations is created, $\mathbf{A}(r,\theta,\varphi,T_i,\tau^j_C\Delta G^j_i).X = y$ where $\mathbf{A}$ is the matrix of coefficients for each voxel (row) and spherical harmonic coefficients (column); X is a vector containing the unknowns weights a^j_{nm} and b^j_{nm}; and, y are the measured eddy current field estimates for each voxel using the different diffusion-weighting gradient amplitudes applied along the principal axes. The linear system of equations was solved using linear least squares minimization and was repeated for each gradient coil. Once the weights a^j_{nm} and b^j_{nm} are known for each gradient coil, (4) can be evaluated to predict an eddy current field map image, given any diffusion-weighted protocol, required by any of the available field map EPI distortion correction software.

TABLE II
IMAGE ACQUISITION PARAMETERS

Acquisition parameters for:	Phantom field maps		In-vivo validation		
	2D	3D	Clinical		High b-value
TE (ms)	20	20	102	91	119
TR (ms)	1000	150	4800		4800
Matrix size	64	32	84		128
Voxel size (mm)	6x6x6	8x8x8	2.5x2.5x3		1.7x1.7x2.0
Slices	1		32		30
Slice gap (mm)			0		1
GRAPPA			2		2
BW (Hz/pixel)	130	390	1384		1954
τ_{ES} (ms)			0.81		0.76
PFR			6/8		6/8
T_{acq} (min:s)	1:08	5:08	1:08		5:22
δ (ms)			37.8	32.3	42.4
Δ (ms)			47.3	41.8	57.0
b-value (s/mm^2)			1000		3000
No of. Directions			12		64

D. In Vivo Acquisition

To verify the eddy current characterization and the ability to predict eddy current related geometric distortion *in vivo*, four normal subjects were acquired with two typical clinical protocols. The clinical protocols consisted of a b-value of 1000 s/mm^2 scans applied with 12 different directions, distributed isotropically on a sphere. The TE of the first ST DW gradient acquisition was initially matched to what could be achieved with the EC insensitive TRSE DW gradients, the TE of the second acquisition used the minimum possible TE achievable with the use of ST DW gradients. To show the potential of this method at high b-values, a single subject was imaged with a b-value of 3000 s/mm^2 using 64 different directions distributed isotropically on a sphere. In addition, the images were acquired off isocenter to ensure that slices containing the white matter tracts would experience significant eddy current induced geometric distortions. The other image parameters, including the diffusion-weighting gradient duration (δ) and separation times (Δ), are given in Table II.

The *in vivo* examples we present in this work used (4) to predict the field maps and corrected the geometric distortions using FSL's FUGUE EPI Unwarping toolbox [31]. FSL's "eddy_correct," which includes bulk motion correction, was also applied for comparison. Because an image registration based correction also corrects for rigid body motion, the fieldmap correction was also corrected for rigid body motion by registering the images to the b-0 image. Similarly the TRSE method was also registered to the b-0 Stesjkal–Tanner image to correct for rigid body motion using FSL's Flirt algorithm. The effect of the distortion

correction were assessed visually by creating a standard deviation map across the directions. Similar to FA, in a standard deviation map voxels at sites presenting isotropic diffusion properties appear hypointense and anisotropic diffusion properties appear, or regions that are distorted, hyperintense [13] but it was found to be a more sensitive measure of correction efficiency when comparing within a b-value shell. At low b-values scans, quantitative verification of improvement is provided by measuring FA values from regions of interest (ROI) at the anterior and posterior edges of the brain, the corpus callosum splenium and in ventricular CSF. The ROI were identified on the uncorrected Stesjkal–Tanner image and translated to the corrected and TRSE images.

To investigate the potential of the correction at high b-values, we compared the fiber orientation distributions (FOD) in each voxel as estimated by the classical constrained spherical deconvolution (CSD) technique [32]. We used the original implementation available in the MRtrix toolbox [33] and a real and symmetric spherical harmonic basis of the eighth order. For the estimation of the single-fiber profile (response function) we followed the guidelines suggested in [32]. Deterministic fiber-tracking was performed using MRtrix's "streamtrack" algorithm with default parameters.

All experiments were performed on a clinical 3T scanner (45 mT/m max gradient) with a 32-channel head coil (MAGNETOM Trio a Tim System, Siemens AG, Healthcare Sector Erlangen, Germany) using manufacturer determined settings.

III. Results

A. Phantom Validation

As the general description of the eddy current field is based on a higher order spherical harmonics (2) we first determined the minimum order required to sufficiently capture the expected spatial dependence [Fig. 2(a)]. The root mean square (RMSE) error of the diffusion-weighting gradient along Z is initially much larger due to a larger constant offset. Once removed, all three gradients are comparable. A second-order spherical harmonic fit (nine degrees-of-freedom) is the minimum required to describe the eddy current field. Increasing the order causes limited improvement in the RMSE. We determined that a third-order spherical harmonic fit, which results in a residual RMSE of ~ 1 Hz on the principal axes, was a sufficient compromise between accuracy and model complexity and will be used for further analysis.

To validate the use of a single eddy current decay time constant (1) as a fair approximation of the eddy current field's behavior, Fig. 2(b) plots the eddy current field from a diffusion-weighting gradients applied along each of the principal axis as a function of delay time. A strong mono-exponentially decaying relationship was shown for each gradient axis over the time period measured. No spatial dependence was observed. The time constants for the X, Y, and Z gradient axis were found to be of 80.3, 62.1, and 79.8 ms, respectively. With these time constants, the gradient ramps from the second preceding TR would found to contribute weights of $< 2\%$ and were thus neglected. Only gradient ramps from the current and previous TR were considered in (4).

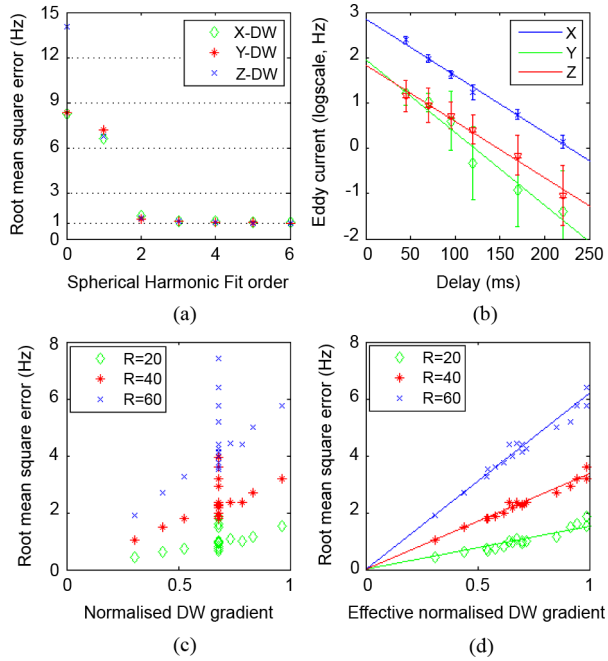

Fig. 2. Validation of model assumptions. The residual RMSE of the eddy current field, for each of the three diffusion-weighting gradients, b-value $2000\,\mathrm{s/mm^2}$ aligned along the principal axis, reduces with the order of the spherical harmonic fit (a). Image (b) shows the expected linear trend between the mean of the log(RMSE) as a function of delay. Images (c) and (d) plot the raw root mean square error of the eddy current field, aligned along the X-axis, from three surfaces of different radii (20, 40, and 60 mm) against the normalized diffusion-weighting gradient amplitude (c) and the effective normalized gradient amplitude (d) predicted by (1). Normalized diffusion-weighting gradient amplitude can only model protocols where the gradient shape, the TR or delay do not change; however applying linear response theory enables the model to be predictive of these changes to the protocol.

To illustrate the need to consider all diffusion-weighting parameters, Fig. 2(c) and (d) plots the raw RMSE of the eddy current field from three surfaces of different radii (20, 40, and 60 mm). The eddy current field was larger at higher b-values as expected but protocol changes that result in different timing characteristics can not be captured by a simple dependency on the diffusion-weighting gradient amplitude alone, as shown by the clustering of points in Fig. 2(c). At different gradient shapes, the raw RMSE for each field is similar despite the larger gradients used with the shorter diffusion-weighting gradient pulses. Using linear response theory, by summing the contribution of gradient ramps from two sequence TRs, the linearity is restored across all protocols [Fig. 2(d)].

We found that the raw RMSE of the Z diffusion-weighting gradient is fairly constant as a function of radial location due to a large constant offset observed and raw RMSE of the X and Y diffusion-weighting gradient eddy current fields are larger further from isocenter. The ability to capture oblique diffusion weighted gradient directions based on the characterization of gradients aligned along the principal axes is demonstrated in Fig. 3(a). After subtraction of the eddy current field predicted by (4), the residual RMSE is reduced to < 1 Hz for all experiments where the diffusion-weighting gradient is aligned with the principal axes (data not shown). The oblique diffusion-weighting gradients have a slightly larger residual RMSE than those aligned with the principal axes. The RMSE is < 1.3 Hz for

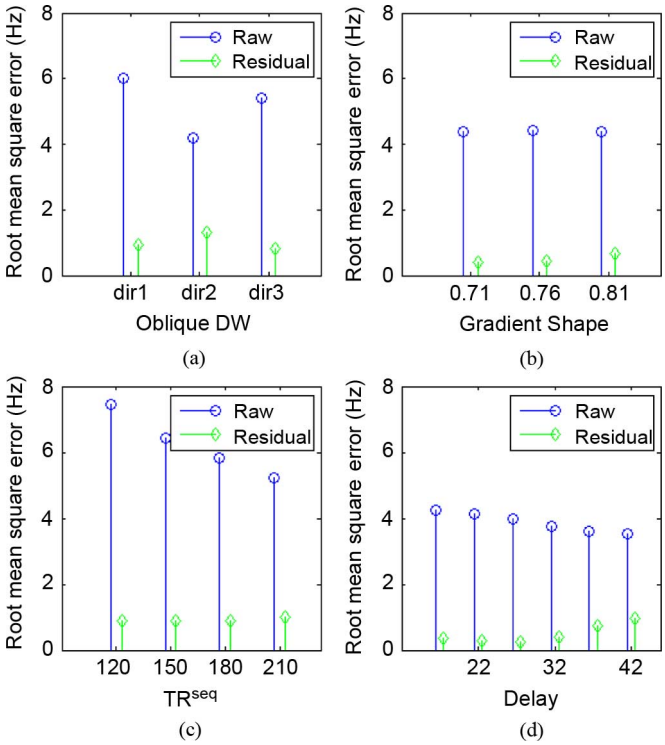

Fig. 3. Raw and residual RMSE from a surface of radius 60 mm. A model, based on the principal directions, is able to predict the induced eddy current field to ~ 1 Hz for a range of different protocol settings. (a) Different oblique diffusion-weighted gradient directions. (b) Gradient shapes. (c) TRSeq. (d) Different delays.

the oblique diffusion-weighting gradients while the RMSE is < 0.3 Hz for diffusion-weighting gradient aligned with the principal axes with an equivalent b-value of 1000 s/mm^2.

To further validate our assumptions on the effect of timing characteristics of the diffusion-weighting gradients Fig. 3(b)–(d) plots the raw and residual RMSE as a function of gradient shape, TRSeq, and delay. The effect of different gradient shapes shows the raw RMSE is relatively constant despite the diffusion-weighting gradient increasing in amplitude as pulses become shorter [Fig. 3(b)]. As the TRSeq is increased the raw RMSE decreases even though the diffusion-weighting gradient pulse remains the same indicating the eddy current history effect between sequence repetitions [Fig. 3(c)]. At longer delays, the raw RMSE reduces slowly indicating that the eddy current field is dominated by a long-term eddy current component as assumed but for the purposes of distortion correction can be considered time invariant [Fig. 3(d)].

Fig. 4 shows surface representations of the raw (b-value 2000 s/mm^2) and residual eddy current field at a radius of 60 mm. For the oblique diffusion-weighting gradients most of the spatial dependencies of the raw eddy current fields are well captured by the fitted eddy current model but the residual eddy current field shows continued spatial dependence compared to when the diffusion-weighting is applied only along one axis. Fig. 5 shows a comparison between the predicted and fitted spherical harmonic coefficients. When the magnitude of the spherical harmonic coefficient is large, the predicted coefficient agrees well with the fitted. Smaller coefficients show more variation with the fitted eddy current model's coefficients. The small differences between the predicted and fitted spherical harmonic coefficients may explain why some spatial dependency remains in the residual RMSE seen in Fig. 4. Overall the residual RMSE for each oblique diffusion-weighted gradient direction was reduced from 6.0, 4.2, and 5.4 Hz to 0.9, 1.3, and 0.8 Hz over this surface.

B. In Vivo Validation

To assess the characterization of the eddy current field with (4), the ability to remove the geometric distortion *in vivo* was assessed using two typical clinical protocols. After distortion correction with the predicted field maps the misalignments are mostly removed. The standard deviation maps of the diffusion-weighted images acquired using the clinical protocols, with different diffusion-weighted gradients timing characteristics (Table II), are shown in Figs. 6 and 7. The pixel-wise standard deviation maps, across the directions, show eddy current induced misalignment of the uncorrected Stesjkal–Tanner images. Regions of high standard deviations can be seen at the anterior and posterior edges of the brain. After distortion correction with the predicted field maps, the regions of high standard deviation at the edges of the image are reduced in intensity without significant blurring of the image. Further improvement could be obtained after the additional step to correct for rigid body motion was performed. The results obtained with the proposed methodology compare well with FSL's image registration eddy current correction. Qualitatively, the TRSE acquisition outperforms the retrospective correction methods as no high standard deviations are found at the edges of the anatomical image.

For a more quantitative assessment of the residual eddy current contamination, the FA values from each of the four subjects, with the TE 102 ms clinical protocol are presented in Table III. In the Corpus Callosum Splenium where an FA value of 0.7–0.8 is expected, the mean and standard deviation of the FA are unchanged after correction for each subject. Both the mean and standard deviation in the CSF decrease and are similar to TRSE after FSL and fieldmap $+$RB corrections (as in the CSF isotropic diffusion can be assumed FA should be very close to zero); however in the fieldmap only correction the CSF value remains largely unchanged. The ROI for the anterior and posterior images were traced around the areas of hyperintense signal in the standard deviation map of the uncorrected Stejskal–Tanner image. In general, at the anterior and posterior edges of the brain, the mean FA decreases after all applied corrections: FSL, fieldmap, and fieldmap $+$RB corrections; however these values were still at least double what was observed in the TRSE. In the anterior region of subject 1 and 4 and the posterior region of subject 4 the fieldmap correction performs particularly well compared to FSL. In all other regions the fieldmap correction with and without bulk motion correction the mean FA was similar to FSL. In most cases, the standard deviation of the FA is only slightly reduced and indicates the presence of residual errors in each method compared to the TRSE.

The proposed method's potential at high b-values is shown in Fig. 8. Without correction, the high b-value protocol shows regions of poor coherence in the fibers extending from the corpus callosum and the FODs show a lack of coherence on

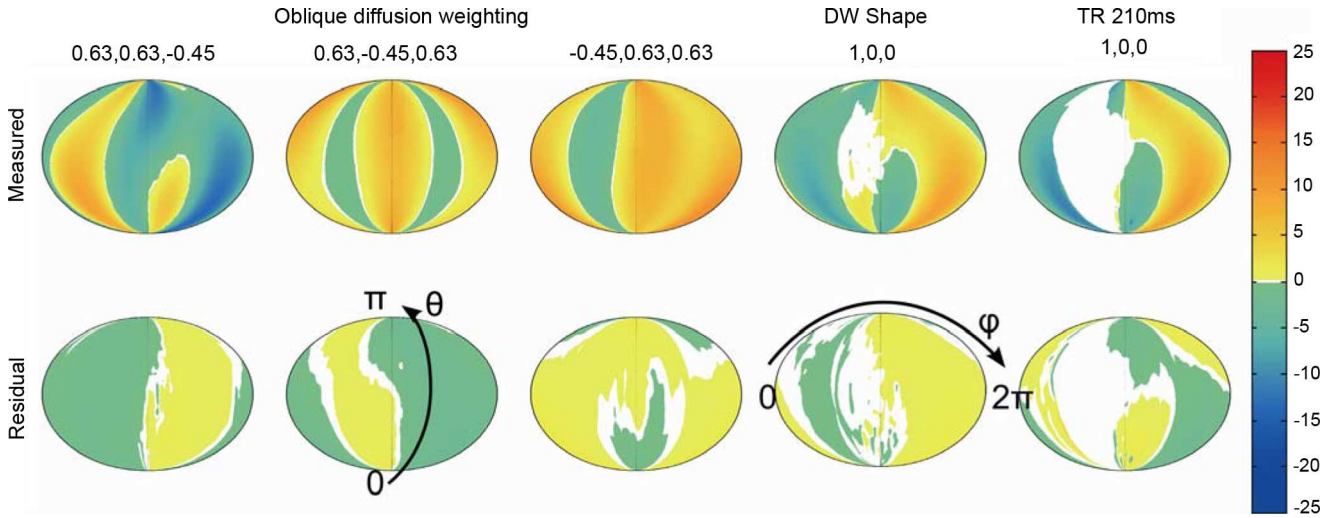

Fig. 4. Surface representations of the raw and residual eddy current fields. The ability to capture spatial dependence in the model is shown by comparing the fitted and predicted eddy current fields induced when using oblique diffusion-weighted gradient directions, the shortest diffusion-weighting gradient pulse shape ($\delta = 29$ ms) and a TR of 210 ms. Color scale represents the strength of the eddy current field (Hz) at the spherical surface of radius 60 mm.

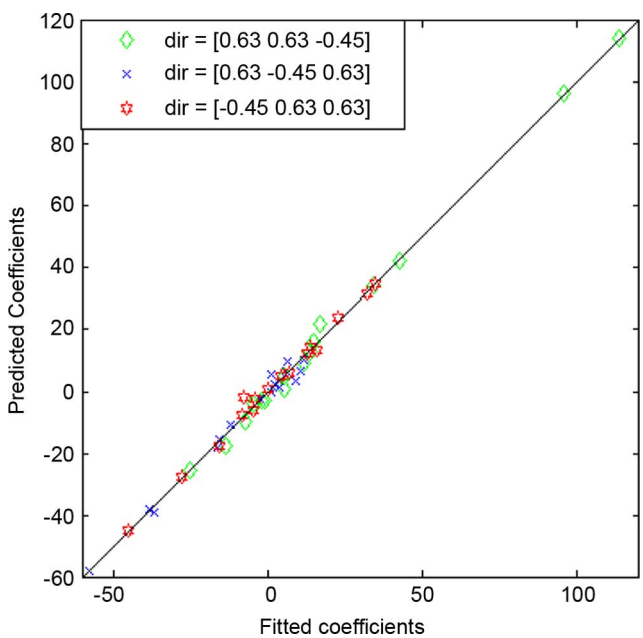

Fig. 5. Comparison of the fitted and predicted spherical harmonic coefficients. The majority of the fitted and predicted coefficients for the three oblique diffusion-weighted gradient directions are in good agreement. The few coefficients that are not well predicted are small in magnitude.

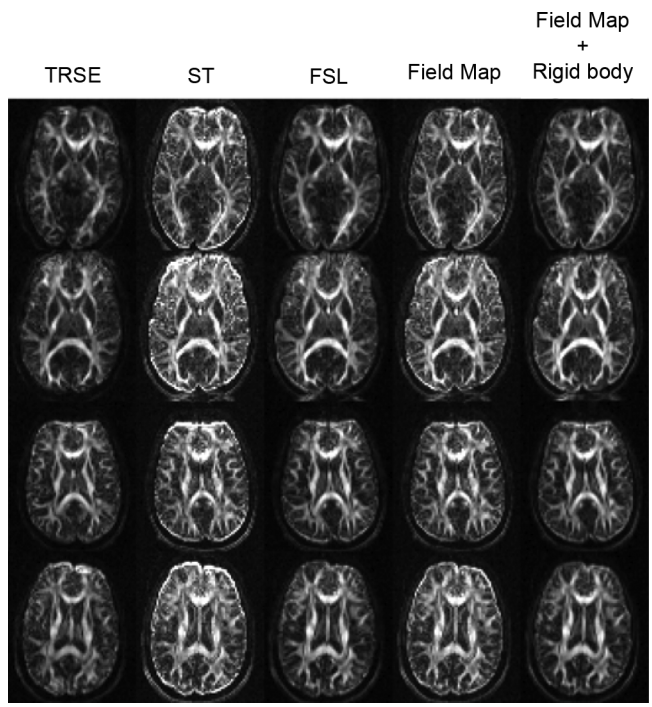

Fig. 6. Standard deviation maps from four subjects using two Stejskal–Tanner (ST) clinical protocols $\mathrm{TE} = 102$ ms ($\mathrm{BW} = 37.4$ Hz/pixel) at different positions (15.0, 18.2, 35.1, and 30.05 mm, respectively). The ST images have been corrected with FSL eddy current distortion algorithm, the predicted field map with and without a rigid body registration with FSL. The twice refocused spin echo (TRSE) is also provided for comparison. The greyscale was fixed across all images and was chosen to emphasize the residual distortion errors seen in the Stejskal–Tanner image after correction. The errors are significantly reduced after distortion correction for each subject, irrespective of the slice location.

the edges of the corpus callosum. This indicates that the major white matter tracts were successfully placed in an eddy current sensitive region as intended. The low SNR remaining at high b-values causes the FSL registration to fail in correcting for the eddy current induced distortions. After FSL correction the coherence of the fibers extending from the corpus callosum was lost. The FODs show that regions of artificial coherence were introduced in the deep gray matter (arrows) by the registration. In comparison the fieldmap +RB correction was not constrained by the low SNR and resulted in an improved coherence of the fibers extending from the corpus callosum and the FODs appear more regular and better represent the underlying anatomy (circles).

IV. Discussion

To remove the necessity of measuring the eddy current field of each diffusion-weighted gradient direction and amplitude for

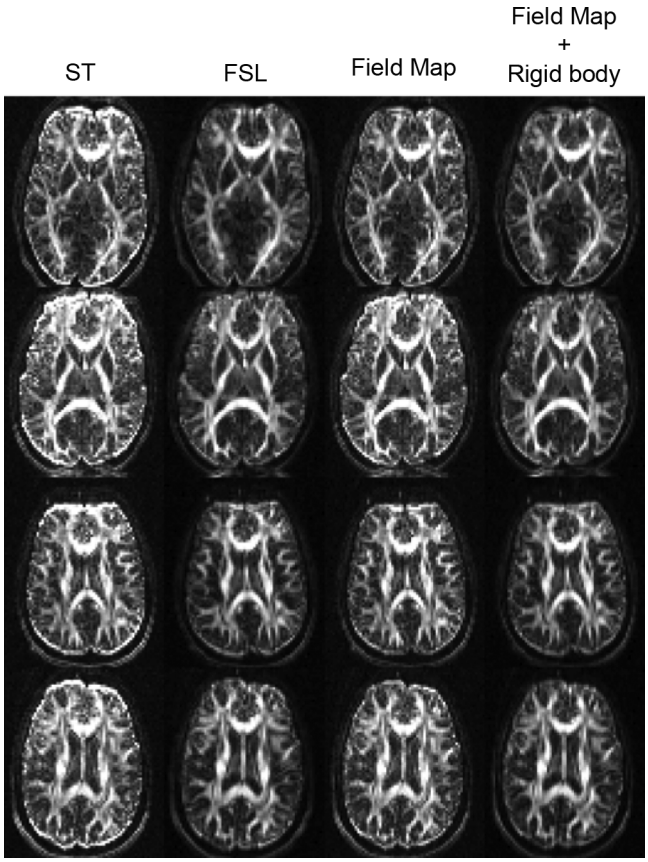

Fig. 7. Standard deviation maps from four subjects using two Stejskal–Tanner (ST) clinical protocols $\mathrm{TE} = 92\ \mathrm{ms}$ $(\mathrm{BW} = 37.4\ \mathrm{Hz/pixel})$ at different positions (15.0, 18.2, 35.1, and 30.05 mm, respectively). ST images have been corrected with FSL eddy current distortion algorithm, the predicted field map with and without a rigid body registration with FSL. Greyscale was fixed across all images and was chosen to emphasize the residual distortion errors of the Stejskal–Tanner image after correction. Errors are significantly reduced after distortion correction for each subject, irrespective of the slice location.

every protocol used, we characterized, using linear response theory, the eddy current field using 2-D and 3-D eddy current field measurements acquired on a phantom to predict the field map required for image-based field map geometric distortion correction.

Eddy current models in the literature [16], [34]–[37] are based on the theoretically constrained linear distortions of scale, shear and translation which approximate the eddy current field as a stack of linear planes. Typical *in vivo* diffusion-weighted EPI acquisitions acquire a stack of transverse slices to achieve coverage of the whole brain, thus the spatial constraint applied in a "correction" based approach is for the eddy current fields to satisfy a smoothly varying function in the (z) direction [38]. Horsfield [36] extends this concept by using a third-order polynomial approximation to improve the in-plane spatial description of the eddy current field; however, this description is "unphysical." Though other basis functions could be utilized, such as a cosine basis functions [39], the use of spherical harmonics provides a generic spatial description of the eddy current field that is based on a physical solution [19] to Laplace's equation. In addition, we found a spherical harmonic fit better described the data than a simple polynomial model [38]. We found that a spherical harmonic fit of order 2, nine degrees-of-freedom, captures the bulk of the eddy current field's spatial dependency. Increasing the order of the fit resulted in limited improvement, as shown in Fig. 2(a). For our scanner, a third-order fit reduced the residual RMSE to less than 1 Hz and was considered a sufficient trade off between accuracy and computational efficiency. Other scanners may have more complicated spatial dependencies and may need to consider higher order fits, which could be determined during the characterization of the system.

The corrected *in vivo* images, had lower FA values and reduced signal variation between diffusion-weighted images at the anterior and posterior edges as shown in Figs. 6 and 7 and in Table III. The inner structures of the brain remained largely unchanged. Without rigid body correction the intensity of the standard deviation map remains similar compared to original Stejskal–Tanner image. After bulk motion correction, the intensity of the fieldmap corrected standard deviation map becomes similar to FSL and the TRSE which also underwent a rigid body registration step. It is well known that an interpolation step blurs the image. The additional improvement seen in Figs. 6 and 7, with the rigid body step was thus in part due to the correction of bulk motion but also the residual errors are dampened by the increased blurring seen in the image. This finding agrees with the FA values which found a similar improvement in the fieldmap correction at the anterior posterior regions of the brain but no improvement of the CSF region, placed in the ventricles, where the eddy current field's geometric distortions are expected to be low.

Fig. 8 demonstrates the advantages of this technique at high b-values where it is known that image registration techniques suffer due to low SNR and distinctly different image features between diffusion directions. The FSL registration over fits the data resulting in regions of false coherence and degrading the coherence present in other regions. In fact, without the availability of an SNR independent correction as proposed, the user would be best not to attempt any eddy current correction at all. In comparison the fieldmap $+\mathrm{RB}$ correction can remove the eddy current distortions and improve the coherence of the FODs and resulting fiber tracking with the underlying anatomy.

Eddy current models have also previously shown that the eddy current field is linearly dependent on the amplitude of the diffusion-weighting gradient. This assumption is a fair approximation if time dependent effects, eddy current history (build up of eddy current across sequence repetitions) and the diffusion-weighting gradient pulses' timing and shape, can be neglected. But, in a clinical setting indirect protocol changes such as image resolution and different partial Fourier ratios may also modify the gradient timing and the induced eddy current field behavior resulting in a loss of linearity with the diffusion-weighting gradient amplitude [Fig. 2(c)]. Through linear response theory, the applicability of the model (4), was extended to cover the temporal characteristics of the eddy current field's behavior Fig. 2(d). This feature removes the requirement to measure the eddy current field map for each specific protocol which currently restricts the usage of field map corrections in a clinical environment. In other words, the proposed correction strategy here requires a one-time characterization of the eddy current field during the scanner tune-up in a fashion as described in materials and methods. The derived

TABLE III
FA VALUES FROM REGIONS OF INTEREST IN TE CLINICAL TE 102 MS PROTOCOL

Subj	Location	TRSE	ST	FSL	Fieldmap	Fieldmap +RB
1	C.C Splenium	0.60 ± 0.15	0.70 ± 0.20	0.66 ± 0.18	0.67 ± 0.18	0.68 ± 0.19
	CSF	0.06 ± 0.02	0.15 ± 0.04	0.07 ± 0.01	0.14 ± 0.04	0.09 ± 0.02
	Anterior	0.06 ± 0.03	0.22 ± 0.10	0.26 ± 0.28	0.14 ± 0.04	0.13 ± 0.05
	Posterior	0.06 ± 0.02	0.40 ± 0.29	0.24 ± 0.24	0.29 ± 0.22	0.24 ± 0.21
2	C.C Splenium	0.78 ± 0.13	0.82 ± 0.15	0.82 ± 0.15	0.81 ± 0.15	0.81 ± 0.16
	CSF	0.05 ± 0.02	0.13 ± 0.03	0.09 ± 0.03	0.13 ± 0.02	0.09 ± 0.03
	Anterior	0.17 ± 0.19	0.45 ± 0.22	0.32 ± 0.28	0.34 ± 0.22	0.30 ± 0.27
	Posterior	0.08 ± 0.04	0.33 ± 0.24	0.31 ± 0.33	0.26 ± 0.20	0.18 ± 0.19
3	C.C Splenium	0.67 ± 0.12	0.76 ± 0.18	0.72 ± 0.17	0.75 ± 0.18	0.72 ± 0.17
	CSF	0.07 ± 0.01	0.17 ± 0.05	0.06 ± 0.03	0.16 ± 0.05	0.08 ± 0.03
	Anterior	0.18 ± 0.18	0.36 ± 0.16	0.32 ± 0.35	0.22 ± 0.11	0.25 ± 0.23
	Posterior	0.11 ± 0.05	0.44 ± 0.30	0.40 ± 0.35	0.35 ± 0.28	0.31 ± 0.30
4	C.C Splenium	0.76 ± 0.16	0.77 ± 0.16	0.78 ± 0.18	0.77 ± 0.16	0.77 ± 0.19
	CSF	0.06 ± 0.01	0.14 ± 0.03	0.10 ± 0.02	0.13 ± 0.03	0.09 ± 0.02
	Anterior	0.14 ± 0.07	0.31 ± 0.16	0.28 ± 0.30	0.21 ± 0.14	0.19 ± 0.20
	Posterior	0.08 ± 0.04	0.29 ± 0.22	0.27 ± 0.31	0.24 ± 0.19	0.15 ± 0.19

eddy current coefficients can then be applied to a wide range of diffusion protocols without any limitations on scanned body region and image properties including SNR and CNR.

On the contrary, the eddy current models presented in the literature, which aim to correct eddy current induced distortions at higher b-values, rely on the ability to reliably extrapolate the image registration parameters as a function of gradient strength [16], [35], [37]. To ensure a linearity of the image registration parameters with gradient strength these models: 1) must have enough reliably registered low b-value scans to obtain the linear fit; 2) have a similarity measure required that minimizes the registration error of images with significantly different features; 3) should not be affected by the compensatory nature of image registration parameters, i.e., image shear can be described using a rotation and translation [40]; and 4) should be independent of the bulk motion. Alternatively, another method attempts to account for the changes in image features between directions by registering the high b-values scans to synthetic images simulated from low b-values [41]. However, this approach again requires additional low b-value scans which increases the acquisition time and assumes that no rigid body motion occurs between the low and high b-value scans. In comparison, the proposed eddy current field map correction approach is independent of these limitations. It provides the ability to predict the eddy current field for any image orientation and can account for changes in the protocols that significantly alter the diffusion-weighting gradients. Furthermore it separates the bulk motion and eddy current correction problems. This would allow a registration with a reduced number of degrees-of-freedom or alternative bulk motion correction strategies [42], [43] to be utilized which should prove more reliable and robust at high b-values.

A. Limitations and Future Work

Susceptibility induced geometric distortion, which is also a major drawback of DW EPI acquisitions could also be incorporated into the correction procedure. For example if a $\overline{EC(x,y,z)}$ B0 fieldmap was available [44], it could be simply added to the predicted fieldmap from the model or after a spherical harmonic fit could be incorporated into (4) as a gradient independent contributor to the predicted fieldmap.

The characterization of the eddy current field was based on measurements from three diffusion-weighted gradient directions applied along each gradient axis, whose amplitudes were equivalent to six different b-values. A total of 48 min was required by the 3-D eddy current field mapping sequence to acquire the diffusion-weighted gradient directions and amplitudes used to determine the unknowns in (4). (The optimization of the field mapping sequence is beyond the scope of this work, but we foresee that great reduction in the scan time is feasible.) A wider, but fewer, selection of diffusion-weighting gradients with different amplitudes and timing characteristics may yield further improvement in the characterization of the eddy current fields. The oblique diffusion-weighted scans showed that the linear superposition of the gradient coils worked well when the spherical harmonic coefficient's spatial dependence was strong. Any significant mismatch between fitted and predicted coefficients occurred when there was a weak dependency. Inclusion of oblique diffusion-weighting gradients in the characterization of the model may further improve the ability to capture all spatial dependencies in the system.

To further reduce the time required to characterize the system a 1-D measurement, similar to the method for evaluating the gradient pre-emphasis unit settings, could equally provide an estimate of the eddy current decay constant rather than the 2-D method applied if no spatial variation of the eddy current decay constant was observed as seen on our system. The number of preceding gradient ramps which need to consider depends on the eddy current field decay constant. On this scanner, consideration of gradient ramps from two sequence repetitions was adequate to obtain the desired linearity, for other scanners with a different eddy current decay constant the model may need to consider

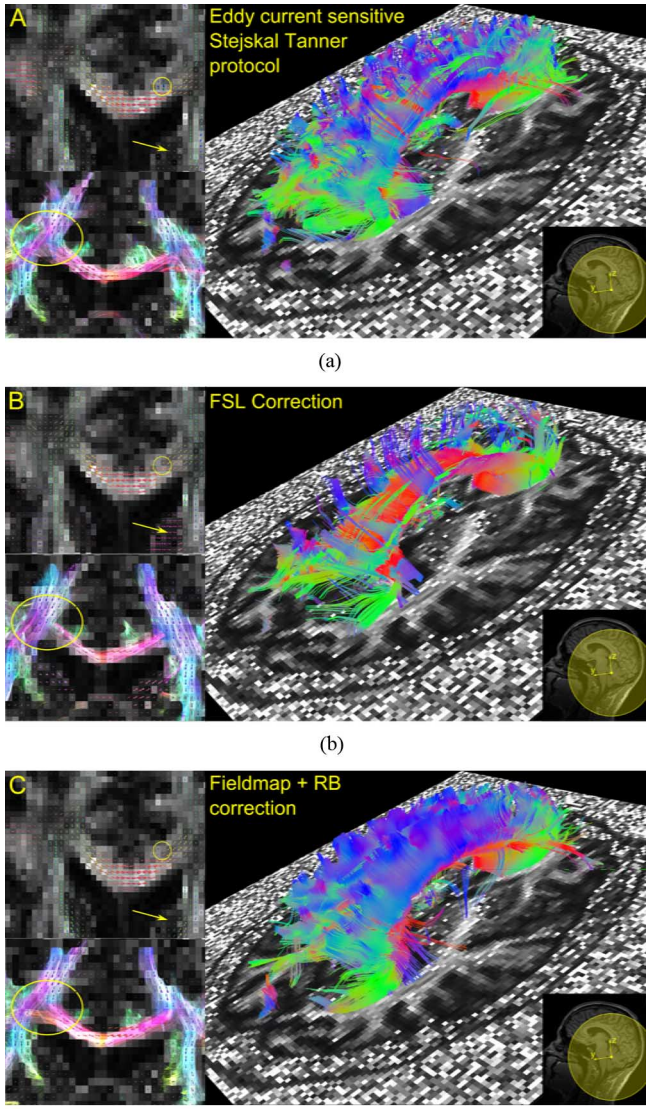

Fig. 8. Distortion correction at high b-values. Eddy current sensitive Stejskal–Tanner protocol was used to acquire the large white matter tracts in an off-center position to ensure significant eddy current induced distortions would occur (A). Insert on the lower right shows the position of isocenter, the outer circle indicates 100 mm from isocenter. An FSL correction (B) failed to recover all fibers extending from the corpus callosum and resulted in false regions of coherence in the deep gray matter (arrow). Fieldmap $+\mathrm{RB}$ (C) correction is able to recover the fibers extending from the corpus callosum, and as shown by the FODs results in an improved coherence in the corpus callosum (small circle) and does not block the extending fibers (ellipse) across all images and was chosen to emphasize the residual distortion errors of the Stejskal–Tanner image after correction. Errors are significantly reduced after distortion correction for each subject, irrespective of the slice location.

the gradient ramps from additional sequence repetitions to satisfactorily capture the eddy current history behavior. It is also important to note that consideration of eddy current history effects allows a truer prediction of the eddy current behavior seen by the first slices of each volume after a change of direction or b-value.

V. Conclusion

We show that using linear response theory to incorporate the diffusion-weighting gradients' timing characteristics and eddy current history allowed the induced eddy current field to be predicted independent of the protocol settings. This modification allowed characterization of the eddy current field prior to use *in vivo* that sufficiently described the geometric distortion experienced in a *in vivo* diffusion-weighted-EPI image due to any arbitrary applied diffusion-weighting gradient amplitude, direction, slice location or orientation in the volume without limits in terms of SNR and CNR in the *in vivo* image and valid for a large range of image protocol parameter. The corrected images have improved image quality without the need of additional field map measurements or pulse sequence modifications. The proposed correction method was found to be capable to correct eddy current effects equally well as existing state-of-the-art retrospective correction schemes (here FSL was used for comparison). Due to the independency of the proposed methodology on image characteristics (e.g., SNR), it is considered to have particular high potential to be applied for emerging diffusion imaging applications where diffusion-weightings as high as $12000\ \mathrm{s/mm^2}$ are used [45]. Errors due to eddy currents are not limited to diffusion-weighted imaging, following similar methodologies could allow the characterization of the eddy current fields for other MR applications such as phase contrast flow measurements, to be quantified, predicted, and corrected.

Acknowledgment

The authors would like to acknowledge the assistance of Dr. C. Granzeria for assistance with interpretation of the tract based analysis.

References

[1] B. Chapman and P. Mansfield, "Double active magnetic screening of coils in NMR," *J. Phys. D: Appl. Phys.*, vol. 19, pp. L129–L131, 1986.
[2] P. Jehenson *et al.*, "Analytical method for the compensation of eddy-current effects induced by pulsed magnetic field gradients in NMR systems," *J. Magn. Reson.*, vol. 90, pp. 264–278, 1990.
[3] J. J. v. Vaals and A. H. Bergman, "Optimization of eddy-current compensation," *J. Magn. Reson.*, vol. 90, pp. 52–70, 1990.
[4] M. Terpstra *et al.*, "Localized eddy current compensation using quantitative field mapping," *J. Magn. Reson.*, vol. 131, pp. 139–143, 1998.
[5] N. G. Papadakis *et al.*, "Gradient preemphasis calibration in diffusion-weighted echo-planar imaging," *Magn. Reson. Med.*, vol. 44, pp. 616–624, 2000.
[6] P. J. Basser and D. K. Jones, "Diffusion tensor MRI: Theory, experimental design and analysis—A technical review," *NMR Biomed.*, vol. 15, pp. 456–467, 2002.
[7] D. Le Bihan *et al.*, "Artifacts and pitfalls in diffusion MRI," *J. Magn. Reson. Imag.*, vol. 24, pp. 478–488, 2006.
[8] Y. Shen *et al.*, "Correction of high-order eddy current induced geometric distortion in diffusion-weighted echo-planar images," *Magn. Reson. Med.*, vol. 52, pp. 1184–1189, 2004.
[9] D. Gallichan *et al.*, "Reducing distortions in diffusion-weighted echo planar imaging with a dual-echo blip-reversed sequence," *Magn. Reson. Med.*, vol. 64, pp. 382–390, 2010.
[10] T. G. Reese *et al.*, "Reduction of eddy-current-induced distortion in diffusion MRI using a twice-refocused spin echo," *Magn. Reson. Med.*, vol. 49, pp. 177–182, 2003.
[11] O. Heid, "Eddy current-nulled diffusion weighting," in *Proc. 8th Sci. Meeting Int. Soc. Magn. Reson. Med.*, Denver, CO, 2000, pp. 799–799.
[12] E. O. Stejskal and J. E. Tanner, "Spin diffusion measurements: Spin echoes in the presence of a time-dependent field gradient," *J. Chem. Phys.*, vol. 41, pp. 288–292, 1965.
[13] J. Finsterbusch, "Eddy-current compensated diffusion-weighting with a single refocusing RF pulse," *Magn. Reson. Med.*, vol. 61, pp. 748–754, 2009.
[14] J. C. Haselgrove and J. R. Moore, "Correction for distortion of echo-planar images used to calculate the apparent diffusion coefficient," *Magn. Reson. Med.*, vol. 36, pp. 960–964, 1996.

[15] S. Maniega *et al.*, "A quantitative comparison of two methods to correct eddy current-induced distortions in DT-MRI," *Magn. Reson. Med.*, vol. 25, pp. 341–349, 2007.
[16] S. Mohammadi *et al.*, "Correcting eddy current and motion effects by affine whole-brain registrations: Evaluation of three-dimensional distortions and comparison with slicewise correction," *Magn. Reson. Med.*, vol. 64, pp. 1047–56, 2010.
[17] L. R. Arlinghaus *et al.*, "Motion and distortion correction in diffusion-weighted MRI of the breast at 3T," *J. Magn. Reson. Imag.*, vol. 33, pp. 1063–70, 2011.
[18] T. Benner *et al.*, "Diffusion imaging with prospective motion correction and reacquisition," *Magn. Reson. Med.*, vol. 66, pp. 154–167, 2011.
[19] C. Boesch *et al.*, "Temporal and spatial analysis of fields generated by eddy currents in superconducting magnets: Optimization of corrections and quantitiative characterization of magnet/gradient systems," *Magn. Reson. Med.*, vol. 20, pp. 268–284, 1991.
[20] P. Jezzard *et al.*, "Characterization of and correction for eddy current artifacts in echo planar diffwsion imaging," *Magn. Reson. Med.*, vol. 39, pp. 801–812, 1998.
[21] N. G. Papadakis *et al.*, "K-space correction of eddy-current-induced distortions in diffusion-weighted echo-planar imaging," *Magn. Reson. Med.*, vol. 53, pp. 1103–1111, 2005.
[22] B. Chen *et al.*, "Correction for direction-dependent distortions in diffusion tensor imaging using matched magnetic field maps," *NeuroImage*, vol. 30, pp. 121–129, 2006.
[23] T.-K. Truong *et al.*, "Integrated sense DTI with correction of susceptibility- and eddy current-induced geometric distortions," *NeuroImage*, vol. 40, pp. 53–58, 2008.
[24] D. S. Tuch, "Q-ball imaging," *Magn. Reson. Med.*, vol. 52, pp. 1358–1372, 2004.
[25] C. B. Barmet *et al.*, "Spatiotemporal magnetic field monitoring for MR," *Magn. Reson. Med.*, vol. 60, pp. 187–197, 2008.
[26] N. De Zanche *et al.*, "NMR probes for measuring magnetic fields and field dynamics in MR systems," *Magn. Reson. Med.*, vol. 60, pp. 176–186, 2008.
[27] K. M. Vliet, *Linear response theory*. Utrecht, The Netherlands: Rijksuniversiteit, 1977.
[28] K. O'Brien *et al.*, "Robust 3-D eddy current models for geometric distortion correction in diffusion weighted EPI," in *ESMRMB 2011 Congress*, Leipzig, Germany, 2011, p. 333.
[29] M. A. Bernstein *et al., Handbook of MRI Pulse Sequences*. New York: Elsevier Academic Press, 2004.
[30] D. C. Ghiglia and L. A. Romero, "Robust two dimensional weighted and unweighted phase unwrapping that uses fast transforms and iterative methods," *J. Opt. Soc. Am. A*, vol. 11, 1994.
[31] S. M. Smith *et al.*, "Advances in functional and structural MR image analysis and implementation as FSL," *NeuroImage*, vol. 23, pp. 208–219, 2004.
[32] J. D. Tournier *et al.*, "Robust determination of the fibre orientation distribution in diffusion MRI: Non-negativity constrained super-resolved spherical deconvolution," *NeuroImage*, vol. 35, pp. 1459–1472, 2007.
[33] J. D. Tournier *et al.*, "Mrtrix: Diffusion tractography in crossing fiber regions," *Int. J. Imag. Syst. Technol.*, vol. 22, pp. 53–66, 2012.
[34] J. Andersson, "A model-based method for retrospective correction of geometric distortions in diffusion-weighted EPI," *NeuroImage*, vol. 16, pp. 177–199, 2002.
[35] H. Hansson *et al.*, "A novel robust algorithm to correct for eddy current distortions in high b-value diffusion MRI," *Proc. Int. Soc. Magn. Reson. Med.*, vol. 18, 2010.
[36] M. A. Horsfield, "Mapping eddy current induced fields for the correction of diffusion-weighted echo planar images," *Magn. Reson. Imag.*, vol. 17, pp. 1335–1345, 1999.
[37] J. Zhuang *et al.*, "Correction of eddy-current distortions in diffusion tensor images using the known directions and strengths of diffusion gradients," *J. Magn. Reson. Imag.*, vol. 24, pp. 1188–1193, 2006.
[38] K. O'Brien *et al.*, "A 3-D eddy current model for the prediction of geometric image distortions in Stejskal-Tanner diffusion weighted EPI," in *Proc. Int. Soc. Mag. Reson. Med.*, Montreal, Canada, 2011, pp. 3506–3506.
[39] R. Woods *et al.*, "Rapid automated algorithm for aligning and reslicing PET images," *J. Comput. Assist. Tomogr.*, vol. 16, pp. 620–633, 1992.
[40] A. S. Glassner, *Graphics Gems*. San Diego, CA: Elsevier, 1990.
[41] S. Ben-Amitay *et al.*, "Motion correction and registration of high b-value diffusion weighted images," *Magn. Reson. Med.*, vol. 67, pp. 1694–1702, 2012.
[42] R. J. Ordidge *et al.*, "Correction of motional artifacts in diffusion-weighted MR images using navigator echoes," *Magn. Reson. Imag.*, vol. 12, pp. 455–460, 1994.
[43] T. Kober *et al.*, "Prospective and retrospective motion correction in diffusion magnetic resonance imaging of the human brain," *NeuroImage*, vol. 59, pp. 389–398, 2012.
[44] P. Jezzard and R. S. Balaban, "Correction for geometric distortion in echo planar images from B0 field variations," *Magn. Reson. Med.*, vol. 34, pp. 65–73, 1995.
[45] J. Bardin, "Making connections: Is a project to map the brain's full communications network worth the money?," *Nature*, vol. 483, pp. 394–396, 2012.